Letter

Quantum Hall correlations in tilted extended Bose-Hubbard chains

Hrushikesh Sable,* Subrata Das,† and Vito W. Scarola‡
Department of Physics, Virginia Tech, Blacksburg, Virginia 24061, USA

(Received 6 November 2025; accepted 9 January 2026; published 27 January 2026)

We demonstrate characteristics of a bosonic fractional quantum Hall (FQH) state in a one-dimensional extended Bose-Hubbard model (eBHM) with a static tilt. In the large tilt limit, quenched kinetic energy leads to emergent dipole moment conservation, enabling mapping to a model generating FQH states. Using exact diagonalization, density matrix renormalization group, and an analytical transfer matrix approach, we analyze energy and entanglement properties to reveal FQH correlations. Our findings set the stage for the use of quenched kinetics in simple time-reversal invariant eBHMs to explore emergent phenomena.

DOI: 10.1103/2w5f-bh3p

Introduction. Bose-Hubbard models (BHMs) were first constructed to study the quantum liquid phases of helium [1]. They have since been used to model a variety of systems, including helium supersolids [2,3], disordered superconductors [4], Josephson junction arrays [5], photonics-based systems (such as photonic crystal cavities and circuit-QED devices [6–10]), and optically trapped ultracold atoms and molecules [11–15]. Ground states of these models typically follow the Landau paradigm of conventional ordering [16].

Strategies aimed at enriching the phase diagrams of these models beyond the Landau paradigm frequently employ synthetic external fields, implemented in theoretical frameworks or experimental setups [17–28]. Efforts to, for example, construct and study large magnetic field effects on bosons seek to reach the lowest Landau level (LLL) limit where, as Laughlin first pointed out [29], the flat kinetic energy band leads to interaction-only models captured by idealized parent models [30,31]. Here, fractional quantum Hall (FQH) states emerge [32–34]. The Laughlin states [33] defy conventional Landau-paradigm order parameters but are instead defined by a collection of specific features we call FQH correlations: zero-energy ground states [30,31]; robust energy gaps [35]; gaplesss $U(1)$ Luttinger liquid edges [36]; fractionally charged excitations [33]; and ground state degeneracies derived from an interplay of many-body translational symmetry [37] and a dipole (or center-of-mass) symmetry [38]. The ground state degeneracies connect to topological order [39]. For example, a bosonic Laughlin state with a twofold ground state degeneracy arises in its parent model when the magnetic field is tuned to have two magnetic flux quanta per particle, i.e., at FQH filling $\nu_{\mathrm{QH}} = 1/2$.

The Wannier-Stark effect has recently been explored as a seemingly disparate route to enrich the physics of BHMs [40–47]. Motivated by studies of localization and band flattening [48–54], recent work demonstrated that application of a strong static (time-reversal invariant) tilt to the BHM can realize unconventional phases by constraining kinetics and emphasizing interaction induced effects [55], in direct analogy to quenched kinetic energy in the LLL [29]. The constrained kinetics is due to an emergent dipole-conserving symmetry [43,56], analogous to the symmetry generating FQH correlations. These analogies thus suggest [52] the exciting possibility that mappings [Fig. 1(a) depicts the mapping] between parent two-dimensional (2D) FQH models and dipole-conserving one-dimensional (1D) lattice models [38,57–66] might help uncover important but hidden physics in dipole-conserving BHMs.

We connect a 2D FQH model and a dipole-conserving 1D extended Bose-Hubbard model (eBHM), revealing FQH correlations in the latter. While the conventional Landau-paradigm phases, e.g., density waves (DWs), have been studied in the 1D eBHM [67,68], we demonstrate that the 1D eBHM with a tilt reveals FQH correlations wherein the ground state adiabatically connects to a Laughlin state [38,69]. We use exact diagonalization (ED) [70] and density matrix renormalization group (DMRG) [71–74] techniques for numerical simulations, and a matrix product state (MPS) wave function [64,65] to analytically compute ground state entanglement properties and make observable predictions toward this emergent quantum phase. Our work thus introduces a surprisingly simple route to realize an FQH correlated state that complements existing approaches in photonic systems [18,19,21,26], superconducting qubits [75–77], and ultracold atoms [17,24,25,78,79]. Our results provide a unifying perspective on a diverse set of topics, connecting topological quantum phases of matter, such as FQH states, with dipole-conserving BHMs. We summarize by proposing directions to generalize the connection between FQH models and time-reversal invariant BHMs.

Model. We consider the repulsive eBHM on a chain with a spatial tilt at lattice filling $\nu_{\mathrm{L}} = 1/2$,

$$\hat{H}_{\mathrm{eBH}} = \sum_{j=1}^{N_s} \frac{U}{2}\hat{n}_j(\hat{n}_j - 1) + \frac{V}{2}\hat{n}_j\hat{n}_{j+1} + \Delta j\hat{n}_j - J(\hat{b}_j^{\dagger}\hat{b}_{j-1} + \mathrm{H.c.}), \quad (1)$$

*Contact author: hsable@vt.edu
†Contact author: subrata@vt.edu
‡Contact author: scarola@vt.edu

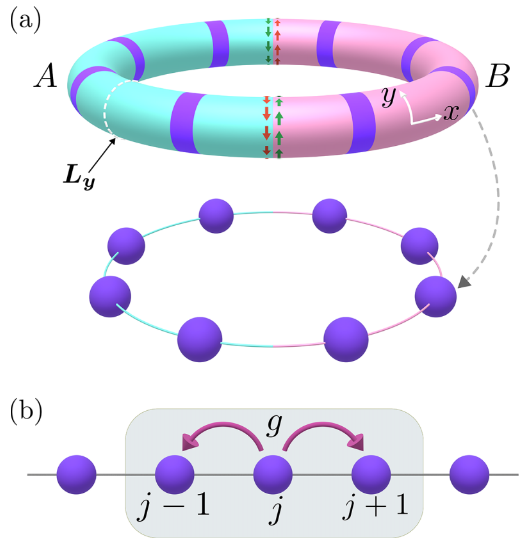

FIG. 1. (a) Top: Bosons on a 2D periodic surface in a strong magnetic field perpendicular to the surface (not shown). The circumference is L_y. LLL single-particle orbitals are drawn as ribbons localized along the x direction. A bipartition separates the system into subsystems A and B used in entanglement calculations. The arrows at the edges of bipartitions depict FQH edge currents. Bottom: A dipole-conserving lattice model where each site (sphere) is mapped from a corresponding FQH orbital in the top. A similar bipartition divides the lattice. (b) Depiction of the dipole-conserving double hop of two bosons to neighboring sites.

where $\hat{b}_j^\dagger$ creates a boson at lattice site j, J is the single-particle hopping energy, $U(V)$ is the on-site (nearest-neighbor) interaction energy, Δ is the tilt strength, and N_s denotes the number of sites.

We expand Eq. (1) in the strong tilt limit, $\Delta \gg J$ and $\Delta \gg U > V$, using the Schrieffer-Wolff transformation [56]. We set $V/U = 2J^2/\Delta^2$ and introduce a gauge transformation on bosonic operators, $\hat{a}_j \equiv i^{j \bmod 2}\hat{b}_j$, to obtain a Hamiltonian valid up to $O[(J/\Delta)^3, (U/\Delta)^3]$ (proven in Supplemental Material Sec. I [80]),

$$\hat{H}_g = \sum_j \left[\hat{n}_j(\hat{n}_j - 1) + 2g(g+3)\hat{n}_j\hat{n}_{j+1} + g^2\hat{n}_j\hat{n}_{j+2} + \left(g\,\hat{a}_j^\dagger\hat{a}_{j+1}^2\hat{a}_{j+2}^\dagger - g^2\,\hat{a}_{j-1}^\dagger\hat{a}_j\hat{a}_{j+1}\hat{a}_{j+2}^\dagger + \text{H.c.}\right)\right], \quad (2)$$

where the gauge transformation gives a positive dipole hopping term [the second to last term as depicted in Fig. 1(b)] with strength $g \equiv 2J^2/(\Delta^2 - 2J^2)$. Importantly, $\hat{H}_g$ commutes with the dipole-moment operator $\hat{P} = \sum_j j\hat{n}_j (\text{mod}\, N_s)$. We therefore consider Eq. (2) as projected into individual dipole moment sectors, thus allowing omission of the constant tilt term and use of periodic boundary conditions.

Equation (2) has another important symmetry, $[\hat{H}_g, \hat{T}] = 0$, where $\hat{T} = \prod_{j=1}^{N_s} \hat{T}_j$ is a many-body translational operator, and $\hat{T}_j$ translates a particle at site j by one site to the right. $\hat{T}$ is of the same form as the symmetry [37] underlying topological order in Laughlin states [39] and establishes a FQH-like algebra, $\hat{U}\hat{T} = \exp(2\pi i\nu_{\text{L}})\hat{T}\hat{U}$, where $\hat{U} \equiv \exp(2\pi i\hat{P}/N_s)$. The phase factor arising from the analogous FQH algebra is, for comparison, $\exp(2\pi i\nu_{\text{QH}})$ [38]. Because $\hat{T}$ and $\hat{U}$ both commute with $\hat{H}_g$ but do not commute with each other, for $\nu_{\text{L}} = 1/2$, both $|\psi_g\rangle$ and $\hat{T}\,|\psi_g\rangle$ have different eigenvalues of $\hat{U}$, leading to a twofold degenerate ground state sector [38,81], analogous to $\nu_{\text{QH}} = 1/2$ FQH models. The existence of these symmetries in $\hat{H}_g$ establishes underlying conditions for FQH correlations, as we argue next.

We compare the low-energy properties of Eq. (2) to a 2D FQH parent model [30,63] of bosons with a repulsive delta function interaction on a thin cylinder of circumference L_y and periodic boundaries at $\nu_{\text{QH}} = 1/2$,

$$\hat{H}_{\text{QH}} = \sum_{j=1}^{N_s} \sum_{k \geqslant |m|} e^{-\frac{2\pi^2(k^2+m^2)}{L_y^2}} \hat{B}_{j+m}^\dagger \hat{B}_{j+k}^\dagger \hat{B}_{j+m+k} \hat{B}_j, \quad (3)$$

where $\hat{B}_j^\dagger$ creates a boson in LLL orbital j [see Fig. 1(a), and Supplemental Material Sec. II [80] for a review].

The matrix elements are exponentially suppressed in $1/L_y^2$ and thus allow expansion by a small parameter. To see how the small parameter arises, note that a single-particle LLL basis state can be written as a product of a plane wave around the circumference (y direction) and a Gaussian along the length (x direction), $e^{i(2\pi k/L_y)y}\phi_m(x)$, where k is an integer and $\phi_k(x) \sim \exp[-(x + 2\pi k/L_y)^2/2]$. The strength of the FQH Hamiltonian matrix elements is then determined by the overlaps between nearest-neighbor basis states along x, $|\langle\phi_k(x)|\phi_{k\pm1}(x)\rangle|^2 \sim \exp(-4\pi^2/L_y^2)$, which yields a small parameter for low L_y. For large L_y, the ground states of $\hat{H}_{\text{QH}}$ become the bosonic Laughlin state [60].

Remarkably, the first four terms of Eq. (2) are nearly the same as the four lowest-order terms of Eq. (3) (Sec. II of Supplemental Material [80]). The coefficient of the nearest-neighbor interaction term in Eq. (2) differs from the FQH model and the last term in Eq. (2) is qualitatively distinct; otherwise they are the same. This shows that $\hat{H}_g$ has the form of a short-ranged FQH-like model. To equate the matrix elements of both models, we make the assignment $g \to 2\exp(-4\pi^2/l^2)$, where l is an artificial length parameter, in Eq. (2). By inserting l, we quantitatively connect a *length* scale in a 2D FQH model (circumference, L_y) to *internal parameters* in $\hat{H}_g$ (the ratio of energy scales captured by l). Conversely, the internal parameters of $\hat{H}_g$ can be used to study the length scaling in FQH models. As both J and Δ are highly controllable in synthetic quantum systems such as cold atoms in optical lattices, tuning g is feasible.

Spectral Structure. We compare properties of eigenstates of Eqs. (2) and (3) in finite-size systems. As expected from Eq. (3), we first checked that Eq. (2) has two zero-energy ground states for low g, using ED and DMRG for up to 32 particles. At high g, while the degeneracy is still two, there are small deviations from zero energy due to the last term in Eq. (2). This confirms a twofold degenerate ground state and energy gap (Sec. I of Supplemental Material [80] presents additional charge gap data). These findings are consistent with generic requirements [81] in lattice models at $\nu_L = 1/2$.

To see the impact of differences between Eqs. (2) and (3), we simulate moderate to large g values. Figure 2 shows example data comparing energy spectra of Eqs. (2) and (3) for moderately high g, $g = 0.8$. As noted earlier, the ground state is marginally lowered below zero, by $\sim 10^{-2}$, implying

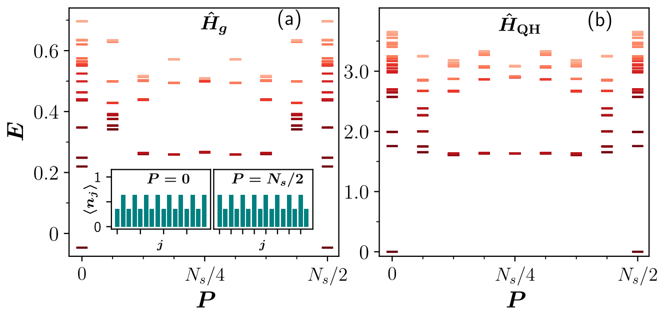

FIG. 2. (a) Low-lying energy eigenvalues of $\hat{H}_g$ vs dipole moment eigenvalue, P, at $g = 0.8$ for $N_s = 16$. Here, we see the ground state degeneracy between P sectors and the energy gap. The insets depict the density profile for the ground states in $P = 0$ and $P = N_s/2$ sectors. (b) The same but for $\hat{H}_{\rm QH}$ at $L_y = 6.5$.

that the correction in energy is an order of magnitude smaller than g. There are other changes to the excitation spectra. For instance, comparing Figs. 2(a) and 2(b), we see that the $P = 1$ excitation sector is higher for Eq. (2). Nonetheless, we have checked that the spectra remain qualitatively similar as we tune g.

Ground State as an MPS. We now focus on ground state properties. Figure 3 shows the overlap, $|\langle\psi_g|\Psi_{L_y}\rangle|$, between the ground state of Eq. (3), $|\Psi_{L_y}\rangle$, and the ground state of Eq. (2), $|\psi_g\rangle$, computed using ED. The solid line depicts the path obtained by equating l and L_y to best approximate the matrix elements of both models. Along this line, we find significant overlaps, nearly 90% and higher, for $L_y \lesssim 7$. The overlap starts to decrease at large g because higher-order terms in Eq. (3) and the last term in Eq. (2) differ. We note that the gauge prescription used to make the dipole hopping term positive is crucial for a nonzero overlap. This implies that $|\psi_g\rangle$ features FQH correlations up to this gauge transformation.

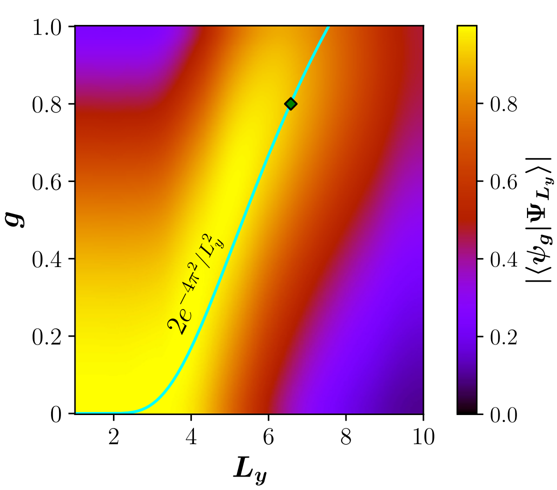

FIG. 3. Overlap between the ground states of $\hat{H}_g$ and $\hat{H}_{\rm QH}$ as we vary dipole hopping strength in $\hat{H}_g$ against the torus circumference in the FQH parent model, for $N_s = 16$. The solid line denotes the parameter choice where the lowest-order terms in each model match. The diamond denotes an example parameter $g = 0.8$ choice that yields an overlap of 90%.

The ground state of Eq. (2) can, in the absence of the g^2 hopping term, be written as an MPS [64]:

$$|\psi_g\rangle_{\rm MPS} = \prod_j \left[1 - \frac{g}{\sqrt{2}}\hat{a}_{j-1}(\hat{a}_j^\dagger)^2\,\hat{a}_{j+1}\right]|101010\ldots\rangle. \quad (4)$$

This wave function is equivalent to a bosonic Laughlin state [65] up to linear order in g. $|\psi_g\rangle_{\rm MPS}$ allows analytic computation of correlation functions with the transfer matrix method.

Correlation functions based on the density reveal a DW phase featuring quantum correlations. $|\psi_g\rangle_{\rm MPS}$ and our numerical results for $|\psi_g\rangle$ on finite-size systems show oscillating density order, as in Fig. 2. We also find that density-density fluctuations, $\langle n_j n_{j'}\rangle - \langle n_j\rangle\langle n_{j'}\rangle$ decay exponentially with $|j - j'|$, consistent with expectations of a gapped 1D quantum phase [82] (Sec. III of Supplemental Material [80] provides numerical data). However, this DW has key differences from ordinary DWs. Most prominently, the eigenstates of Eq. (2) have zero dipole moment fluctuations, $\langle\hat{P}^2\rangle - \langle\hat{P}\rangle^2 = 0$ arising from FQH symmetries, whereas conventional DWs studied in typical eBHMs [e.g., Eq. (1) with $\Delta = 0$ [67]] have $\langle\hat{P}^2\rangle - \langle\hat{P}\rangle^2 \neq 0$. Section IV of Supplemental Material [80] shows an example comparison. Dipole moment fluctuations, therefore, offer an observable that distinguishes dipole-conserving ground states from conventional DWs.

Bipartite Entanglement and Density Fluctuations. We now characterize the entanglement properties of $\hat{H}_g$ ground states. The substitution $g \to 2\exp(-4\pi^2/l^2)$ allows us to also examine the scaling of entanglement properties with l in direct comparison with conventional studies of entanglement that typically probe system-size (length scale) dependence [83]. We start with the entanglement spectrum (ES).

The ES $\{\xi_n\}$ is defined in terms of the pure state Schmidt decomposition of the ground state: $\sum_n e^{-\xi_n/2}|\psi_n^A\rangle \otimes |\psi_n^B\rangle$. The states $|\psi_n^A\rangle$ ($|\psi_n^B\rangle$) form an orthonormal basis for subsystem A (B) due to the bipartition, depicted in Fig. 1(a). The ES can also be labeled with a quantum number defined by the dipole-moment eigenvalue for partition A, $P_{\rm A}(\mathrm{mod}\, N_s/2)$ [62,84].

The inset of Fig. 4(a) plots the ES against $\Delta P_{\rm A}$, the deviation in dipole moment from the“vacuum” state defined as $|101010\ldots\rangle$. The two largest eigenvalues arise from the last (correction) term in $\hat{H}_g$. Otherwise, the remaining four lowest levels form a diamond where the ES of $\hat{H}_g$ and the FQH model match. To understand the four-level diamond ES structure, we start with $|\psi_1^A\rangle$, the state adiabatically connected to the vacuum state with eigenvalue ξ_1 near zero. Removing or adding an edge particle to $|\psi_1^A\rangle$ creates two degenerate dispersing modes, with energies ξ_2 and ξ_3 that arise at $\Delta P_{\rm A} = \pm 1$ [these map to the linearly dispersing edge modes in the FQH model depicted as edge currents in Fig. 1(a)]. The fourth state, with energy ξ_4, can be thought of as a combination of these dispersing modes so that the energy is roughly the sum of the energies of both dispersing modes and the $\Delta P_{\rm A}$ combine to cancel, leaving $\Delta P_{\rm A} = 0$. The diamond structure is therefore consistent with the conformal tower structure of edge Tomonaga-Luttinger liquids seen for FQH models [62,65]. Note that the edge of $\hat{H}_g$ is just a single lattice site but is nonetheless characterized by FQH-like edge current ES with l.

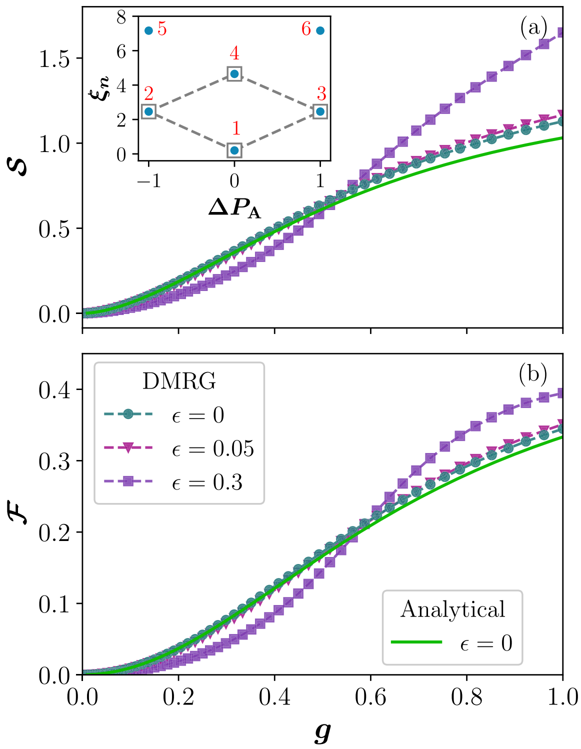

FIG. 4. (a) Entanglement entropy vs g, showing both DMRG data (symbols) for the ground state of $|\psi_g\rangle$ and analytical result from $|\psi_g\rangle_{\text{MPS}}$ (solid line) for $N_s = 64$. The inset depicts the ES, ξ_n, vs dipole moment difference for the ground state of $\hat{H}_{\text{QH}}$ (open squares) and the ground state of $\hat{H}_g$ (solid circles) for $g = 0.5$, and adjacent numbers represent n. The dashed lines are a guide. (b) The same, but for the bipartite number fluctuations.

We use $|\psi_g\rangle_{\text{MPS}}$ to derive the ES. Section V of Supplemental Material [80] reports the full formulas. Expanding about $g = 0$ up to $O(g^3)$ yields $\xi_1 \sim g^2$, $\xi_2 = \xi_3 \sim \ln(2) - 2\ln(g) + 2g^2$, and $\xi_4 \sim 2\ln(2) - 4\ln(g) + 3g^2$. Taking $g \to 2\exp(-4\pi^2/l^2)$ shows that the ES diamond has a height $\xi_4 - \xi_1 = \ln(4) + 16\pi^2 l^{-2} + O[\exp(-1/l^2)]$, where the l^{-2} term shows the leading-order impact of entanglement as the eBHM hopping increases (or, similarly, as the FQH torus diameter is enlarged). The quadratic scaling of ξ_1 with g manifests in other entanglement quantities as well.

We also compute the entanglement entropy: $\mathcal{S} = \sum_n \xi_n e^{-\xi_n}$ [83]. Figure 4(a) compares $\mathcal{S}$ for $|\psi_g\rangle$, and the analytic result obtained from $|\psi_g\rangle_{\text{MPS}}$ (see Sec. V of Supplemental Material [80] for the full functional form of $\mathcal{S}$), and we see excellent agreement. Since $|\psi_g\rangle_{\text{MPS}}$ is equivalent to a bosonic Laughlin state at linear order in g, the agreement of the numerical data of $\hat{H}_g$ with analytics reiterates the FQH correlations in $\hat{H}_g$. Some deviations occur at large g due to the last term in Eq. (2). Furthermore, we have checked that $\mathcal{S}$ for Eq. (3) is identical to within 3% for $g \lesssim 0.8$.

We extract the asymptotic scalings of the entanglement entropy using $|\psi_g\rangle_{\text{MPS}}$. We find that the g^2 and $\ln(g)$ scaling in ξ_n appear such that $\mathcal{S}(g) = g^2[1 + \ln(2) - \ln(g^2)] + O(g^4)$. For $l \to 0$, we find a vanishing entanglement entropy, $\mathcal{S} \to \exp(-8\pi^2/l^2)[1 + \ln(2) + 8\pi^2/l^2)]$, consistent with the vanishing entanglement on a thinning FQH torus model. We find that the large and small l limits of $\mathcal{S}$ saturate to constants, which is also consistent with a theorem establishing area law bounds on the entanglement entropy for gapped short-range 1D spin models [85]. The saturation contrasts with known 2D area law scalings of entanglement entropy, $\sim cl$, where c is a constant [83].

The scaling of the entanglement spectrum and entropy can be connected with observables [86,87]. We compute the bipartite number fluctuations of subsystem A defined as $\mathcal{F} = \langle(\hat{N}_A - \langle\hat{N}_A\rangle)^2\rangle$, with the expectation value taken with respect to the ground state [86]. We find $\mathcal{F}(g) = g^2 + O(g^4)$, which results from the g^2 scaling found in ξ_1.

To check the robustness of these predictions, we introduce ϵ: $V/U = 2J^2/\Delta^2 + \epsilon$. Since $\hat{H}_g$ is derived for $\epsilon = 0$, a nonzero ϵ perturbs all the terms of $\hat{H}_g$ (proven in Sec. VI in the Supplemental Material [80]). Figure 4 shows that ϵ does not change the predictions for $\mathcal{S}$ and $\mathcal{F}$ as long as it is well below the energy gap. The scaling of the observable $\mathcal{F}$ with g can therefore be used to verify the predicted thin torus FQH scaling of $\mathcal{S}$ with g in the eBHM.

Outlook. We demonstrate FQH correlations hidden in strongly tilted 1D eBHMs. Future work shall examine other possible emergent properties imposed by tilt including searches for a nontrivial Zak phase [88,89], calculations done at different fillings to explore the concept of vortex attachment [34,90], and a possible analog to the bosonic Moore-Read state [91,92] at $\nu_L = 1$. It would also be interesting to establish bounds on the minimal number of longer-range interaction terms needed in the 1D eBHM to observe a topological parameter scaling, $\sim c\,l + \gamma$, where γ is topological entanglement entropy, and has value $\log(d)$ where d denotes the ground state degeneracy [93–95]. In addition, higher-dimensional eBHMs might reveal similar FQH correlations by connecting 4D FQH models [96,97] to eBHMs with time reversal invariant fields.

Acknowledgments. H.S. thanks Loïc Herviou for useful discussions. We acknowledge support from AFOSR (Grants No. FA9550-19-1-0272, No. FA2386-21-1-4081, and No. FA9550-23-1-0034) and Army Research Office (ARO) (Grant No. W911NF2210247).

Data availability. The data that support the findings of this article are openly available [98].

[1] T. Matsubara and H. Matsuda, A lattice model of liquid Helium, I, Prog. Theor. Phys. **16**, 569 (1956).

[2] H. Matsuda and T. Tsuneto, Off-diagonal long-range order in solids, Prog. Theor. Phys. Suppl. **46**, 411 (1970).

[3] K.-S. Liu and M. E. Fisher, Quantum lattice gas and the existence of a supersolid, J Low Temp Phys **10**, 655 (1973).
[4] M. P. A. Fisher, P. B. Weichman, G. Grinstein, and D. S. Fisher, Boson localization and the superfluid-insulator transition, Phys. Rev. B **40**, 546 (1989).
[5] C. Bruder, R. Fazio, and G. Schön, The Bose-Hubbard model: From Josephson junction arrays to optical lattices, Ann. Phys. **517**, 566 (2005).
[6] M. J. Hartmann, F. G. S. L. Brandão, and M. B. Plenio, Strongly interacting polaritons in coupled arrays of cavities, Nat. Phys. **2**, 849 (2006).
[7] A. D. Greentree, C. Tahan, J. H. Cole, and L. C. L. Hollenberg, Quantum phase transitions of light, Nat. Phys. **2**, 856 (2006).
[8] D. G. Angelakis, M. F. Santos, and S. Bose, Photon-blockade-induced Mott transitions and XY spin models in coupled cavity arrays, Phys. Rev. A **76**, 031805(R) (2007).
[9] M. Hartmann, F. Brandão, and M. Plenio, Quantum many-body phenomena in coupled cavity arrays, Laser Photonics Rev. **2**, 527 (2008).
[10] I. Carusotto, D. Gerace, H. E. Tureci, S. De Liberato, C. Ciuti, and A. Imamoğlu, Fermionized photons in an array of driven dissipative nonlinear cavities, Phys. Rev. Lett. **103**, 033601 (2009).
[11] D. Jaksch, C. Bruder, J. I. Cirac, C. W. Gardiner, and P. Zoller, Cold bosonic atoms in optical lattices, Phys. Rev. Lett. **81**, 3108 (1998).
[12] V. W. Scarola and S. Das Sarma, Quantum phases of the extended Bose-Hubbard Hamiltonian: Possibility of a supersolid state of cold atoms in optical lattices, Phys. Rev. Lett. **95**, 033003 (2005).
[13] M. Lewenstein, A. Sanpera, V. Ahufinger, B. Damski, A. Sen(De), and U. Sen, Ultracold atomic gases in optical lattices: Mimicking condensed matter physics and beyond, Adv. Phys. **56**, 243 (2007).
[14] I. Bloch, J. Dalibard, and W. Zwerger, Many-body physics with ultracold gases, Rev. Mod. Phys. **80**, 885 (2008).
[15] L. Chomaz, I. Ferrier-Barbut, F. Ferlaino, B. Laburthe-Tolra, B. L. Lev, and T. Pfau, Dipolar physics: A review of experiments with magnetic quantum gases, Rep. Prog. Phys. **86**, 026401 (2023).
[16] S. Sachdev, *Quantum Phase Transitions*, 2nd ed. (Cambridge University Press, Cambridge, UK, 2011).
[17] S. Viefers, Quantum Hall physics in rotating Bose–Einstein condensates, J. Phys.: Condens. Matter **20**, 123202 (2008).
[18] R. O. Umucalılar and I. Carusotto, Artificial gauge field for photons in coupled cavity arrays, Phys. Rev. A **84**, 043804 (2011).
[19] A. Nunnenkamp, J. Koch, and S. M. Girvin, Synthetic gauge fields and homodyne transmission in Jaynes–Cummings lattices, New J. Phys. **13**, 095008 (2011).
[20] J. Dalibard, F. Gerbier, G. Juzeliūnas, and P. Öhberg, Colloquium: Artificial gauge potentials for neutral atoms, Rev. Mod. Phys. **83**, 1523 (2011).
[21] R. O. Umucalılar and I. Carusotto, Fractional quantum Hall states of photons in an array of dissipative coupled cavities, Phys. Rev. Lett. **108**, 206809 (2012).
[22] F. Grusdt and M. Höning, Realization of fractional Chern insulators in the thin-torus limit with ultracold bosons, Phys. Rev. A **90**, 053623 (2014).
[23] N. Goldman, G. Juzeliūnas, P. Öhberg, and I. B. Spielman, Light-induced gauge fields for ultracold atoms, Rep. Prog. Phys. **77**, 126401 (2014).
[24] M. Aidelsburger, *Artificial Gauge Fields with Ultracold Atoms in Optical Lattices*, Springer Theses (Springer, Cham, 2016).
[25] N. Goldman, J. C. Budich, and P. Zoller, Topological quantum matter with ultracold gases in optical lattices, Nat. Phys. **12**, 639 (2016).
[26] T. Ozawa, H. M. Price, A. Amo, N. Goldman, M. Hafezi, L. Lu, M. C. Rechtsman, D. Schuster, J. Simon, O. Zilberberg, and I. Carusotto, Topological photonics, Rev. Mod. Phys. **91**, 015006 (2019).
[27] I. Carusotto, A. A. Houck, A. J. Kollár, P. Roushan, D. I. Schuster, and J. Simon, Photonic materials in circuit quantum electrodynamics, Nat. Phys. **16**, 268 (2020).
[28] S. Aghtouman and M. V. Hosseini, Dimerized Hofstadter model in two-leg ladder quasi-crystals, Sci. Rep. **14**, 8782 (2024).
[29] R. B. Laughlin, Quantized motion of three two-dimensional electrons in a strong magnetic field, Phys. Rev. B **27**, 3383 (1983).
[30] F. D. M. Haldane, Fractional quantization of the Hall effect: A hierarchy of incompressible quantum fluid states, Phys. Rev. Lett. **51**, 605 (1983).
[31] S. A. Trugman and S. Kivelson, Exact results for the fractional quantum Hall effect with general interactions, Phys. Rev. B **31**, 5280 (1985).
[32] D. C. Tsui, H. L. Stormer, and A. C. Gossard, Two-dimensional magnetotransport in the extreme quantum limit, Phys. Rev. Lett. **48**, 1559 (1982).
[33] R. B. Laughlin, Anomalous quantum Hall effect: An incompressible quantum fluid with fractionally charged excitations, Phys. Rev. Lett. **50**, 1395 (1983).
[34] J. Jain, *Composite Fermions* (Cambridge University Press, Cambridge, U.K., 2007).
[35] D. Yoshioka, B. I. Halperin, and P. A. Lee, Ground state of two-dimensional electrons in strong magnetic fields and $\frac{1}{3}$ quantized Hall effect, Phys. Rev. Lett. **50**, 1219 (1983).
[36] X. G. Wen, Gapless boundary excitations in the quantum Hall states and in the chiral spin states, Phys. Rev. B **43**, 11025 (1991).
[37] F. D. M. Haldane, Many-particle translational symmetries of two-dimensional electrons at rational Landau-level filling, Phys. Rev. Lett. **55**, 2095 (1985).
[38] A. Seidel, H. Fu, D.-H. Lee, J. M. Leinaas, and J. Moore, Incompressible quantum liquids and new conservation laws, Phys. Rev. Lett. **95**, 266405 (2005).
[39] X. G. Wen and Q. Niu, Ground-state degeneracy of the fractional quantum Hall states in the presence of a random potential and on high-genus Riemann surfaces, Phys. Rev. B **41**, 9377 (1990).
[40] P. M. Preiss, R. Ma, M. E. Tai, A. Lukin, M. Rispoli, P. Zupancic, Y. Lahini, R. Islam, and M. Greiner, Strongly correlated quantum walks in optical lattices, Science **347**, 1229 (2015).
[41] R. Yao, T. Chanda, and J. Zakrzewski, Many-body localization in tilted and harmonic potentials, Phys. Rev. B **104**, 014201 (2021).
[42] X.-Y. Guo, Z.-Y. Ge, H. Li, Z. Wang, Y.-R. Zhang, P. Song, Z. Xiang, X. Song, Y. Jin, L. Lu, K. Xu, D. Zheng, and H. Fan, Observation of Bloch oscillations and Wannier-Stark

localization on a superconducting quantum processor, npj Quantum Inf. **7**, 51 (2021).

[43] E. Lake, M. Hermele, and T. Senthil, Dipolar Bose-Hubbard model, Phys. Rev. B **106**, 064511 (2022).

[44] G.-X. Su, H. Sun, A. Hudomal, J.-Y. Desaules, Z.-Y. Zhou, B. Yang, J. C. Halimeh, Z.-S. Yuan, Z. Papić, and J.-W. Pan, Observation of many-body scarring in a Bose-Hubbard quantum simulator, Phys. Rev. Res. **5**, 023010 (2023).

[45] P. Zechmann, E. Altman, M. Knap, and J. Feldmeier, Fractonic Luttinger liquids and supersolids in a constrained Bose-Hubbard model, Phys. Rev. B **107**, 195131 (2023).

[46] C. Zerba, A. Seidel, F. Pollmann, and M. Knap, Emergent fracton hydrodynamics of ultracold atoms in partially filled Landau levels, PRX Quantum **6**, 020321 (2025).

[47] S. Kim, B. Kang, P. Segura, Y. Li, E. Lake, B. Bakkali-Hassani, and M. Greiner, Multi-particle quantum walks in a dipole-conserving Bose-Hubbard model, arXiv:2511.02343.

[48] M. Schulz, C. A. Hooley, R. Moessner, and F. Pollmann, Stark many-body localization, Phys. Rev. Lett. **122**, 040606 (2019).

[49] E. Van Nieuwenburg, Y. Baum, and G. Refael, From Bloch oscillations to many-body localization in clean interacting systems, Proc. Natl. Acad. Sci. USA **116**, 9269 (2019).

[50] V. Khemani, M. Hermele, and R. Nandkishore, Localization from Hilbert space shattering: From theory to physical realizations, Phys. Rev. B **101**, 174204 (2020).

[51] S. Scherg, T. Kohlert, P. Sala, F. Pollmann, B. Hebbe Madhusudhana, I. Bloch, and M. Aidelsburger, Observing nonergodicity due to kinetic constraints in tilted Fermi-Hubbard chains, Nat. Commun. **12**, 4490 (2021).

[52] S. Moudgalya, A. Prem, R. Nandkishore, N. Regnault, and B. A. Bernevig, Thermalization and its absence within Krylov subspaces of a constrained Hamiltonian, in *Memorial Volume for Shoucheng Zhang* (World Scientific, Singapore, 2022), pp. 147–209.

[53] M. Will, R. Moessner, and F. Pollmann, Realization of Hilbert space fragmentation and fracton dynamics in two dimensions, Phys. Rev. Lett. **133**, 196301 (2024).

[54] P. Zechmann, J. Boesl, J. Feldmeier, and M. Knap, Dynamical spectral response of fractonic quantum matter, Phys. Rev. B **109**, 125137 (2024).

[55] E. Lake and T. Senthil, Non-Fermi liquids from kinetic constraints in tilted optical lattices, Phys. Rev. Lett. **131**, 043403 (2023).

[56] E. Lake, H.-Y. Lee, J. H. Han, and T. Senthil, Dipole condensates in tilted Bose-Hubbard chains, Phys. Rev. B **107**, 195132 (2023).

[57] E. Westerberg and T. H. Hansson, Quantum mechanics on thin cylinders, Phys. Rev. B **47**, 16554 (1993).

[58] E. J. Bergholtz and A. Karlhede, Half-filled lowest Landau level on a thin torus, Phys. Rev. Lett. **94**, 026802 (2005).

[59] A. Seidel and D.-H. Lee, Abelian and non-Abelian Hall liquids and charge-density wave: Quantum number fractionalization in one and two dimensions, Phys. Rev. Lett. **97**, 056804 (2006).

[60] E. J. Bergholtz and A. Karlhede, One-dimensional theory of the quantum Hall system, J. Stat. Mech. (2006) L04001.

[61] E. J. Bergholtz and A. Karlhede, Quantum Hall system in Tao-Thouless limit, Phys. Rev. B **77**, 155308 (2008).

[62] A. M. Läuchli, E. J. Bergholtz, J. Suorsa, and M. Haque, Disentangling entanglement spectra of fractional quantum Hall states on torus geometries, Phys. Rev. Lett. **104**, 156404 (2010).

[63] P. Soulé and T. Jolicoeur, Edge properties of principal fractional quantum Hall states in the cylinder geometry, Phys. Rev. B **86**, 115214 (2012).

[64] M. Nakamura, Z.-Y. Wang, and E. J. Bergholtz, Exactly solvable fermion chain describing a $\nu = 1/3$ fractional quantum Hall state, Phys. Rev. Lett. **109**, 016401 (2012).

[65] Z.-Y. Wang and M. Nakamura, One-dimensional lattice model with an exact matrix-product ground state describing the Laughlin wave function, Phys. Rev. B **87**, 245119 (2013).

[66] J. R. Cruise and A. Seidel, Sequencing the entangled DNA of fractional quantum Hall fluids, Symmetry **15**, 303 (2023).

[67] T. D. Kühner, S. R. White, and H. Monien, One-dimensional Bose-Hubbard model with nearest-neighbor interaction, Phys. Rev. B **61**, 12474 (2000).

[68] M. A. Cazalilla, R. Citro, T. Giamarchi, E. Orignac, and M. Rigol, One dimensional bosons: From condensed matter systems to ultracold gases, Rev. Mod. Phys. **83**, 1405 (2011).

[69] E. H. Rezayi and F. D. M. Haldane, Laughlin state on stretched and squeezed cylinders and edge excitations in the quantum Hall effect, Phys. Rev. B **50**, 17199 (1994).

[70] D. Gaur, H. Sable, and D. Angom, Exact diagonalization using hierarchical wave functions and calculation of topological entanglement entropy, Phys. Rev. A **110**, 043305 (2024).

[71] S. R. White, Density matrix formulation for quantum renormalization groups, Phys. Rev. Lett. **69**, 2863 (1992).

[72] S. R. White, Density-matrix algorithms for quantum renormalization groups, Phys. Rev. B **48**, 10345 (1993).

[73] M. Fishman, S. R. White, and E. M. Stoudenmire, The ITensor software library for Tensor Network calculations, SciPost Phys. Codebases 4 (2022).

[74] M. Fishman, S. R. White, and E. M. Stoudenmire, Codebase release 0.3 for ITensor, SciPost Phys. Codebases 4 (2022).

[75] P. Roushan, C. Neill, A. Megrant, Y. Chen, R. Babbush, R. Barends, B. Campbell, Z. Chen, B. Chiaro, A. Dunsworth, A. Fowler, E. Jeffrey, J. Kelly, E. Lucero, J. Mutus, P. J. J. O'Malley, M. Neeley, C. Quintana, D. Sank, A. Vainsencher, *et al.*, Chiral ground-state currents of interacting photons in a synthetic magnetic field, Nat. Phys **13**, 146 (2017).

[76] A. Kirmani, K. Bull, C.-Y. Hou, V. Saravanan, S. M. Saeed, Z. Papić, A. Rahmani, and P. Ghaemi, Probing geometric excitations of fractional quantum Hall states on quantum computers, Phys. Rev. Lett. **129**, 056801 (2022).

[77] A. Kirmani, D. S. Wang, P. Ghaemi, and A. Rahmani, Braiding fractional quantum Hall quasiholes on a superconducting quantum processor, Phys. Rev. B **108**, 064303 (2023).

[78] N. R. Cooper, J. Dalibard, and I. B. Spielman, Topological bands for ultracold atoms, Rev. Mod. Phys. **91**, 015005 (2019).

[79] J. Léonard, S. Kim, J. Kwan, P. Segura, F. Grusdt, C. Repellin, N. Goldman, and M. Greiner, Realization of a fractional quantum Hall state with ultracold atoms, Nature (London) **619**, 495 (2023).

[80] See Supplemental Material at http://link.aps.org/supplemental/10.1103/2w5f-bh3p for (i) derivations, (ii) review of FQH models, and (iii) additional numerical data and full analytical formulas, which includes Refs. [30,31,34,38,56,58,63–65,70,73,82].

[81] M. Oshikawa, Commensurability, excitation gap, and topology in quantum many-particle systems on a periodic lattice, Phys. Rev. Lett. **84**, 1535 (2000).

[82] M. B. Hastings and T. Koma, Spectral gap and exponential decay of correlations, Commun. Math. Phys. **265**, 781 (2006).

[83] J. Eisert, M. Cramer, and M. B. Plenio, *Colloquium*: Area laws for the entanglement entropy, Rev. Mod. Phys. **82**, 277 (2010).

[84] H. Li and F. D. M. Haldane, Entanglement spectrum as a generalization of entanglement entropy: Identification of topological order in non-Abelian fractional quantum Hall effect states, Phys. Rev. Lett. **101**, 010504 (2008).

[85] M. B. Hastings, An area law for one-dimensional quantum systems, J. Stat. Mech. (2007) P08024.

[86] H. F. Song, S. Rachel, C. Flindt, I. Klich, N. Laflorencie, and K. Le Hur, Bipartite fluctuations as a probe of many-body entanglement, Phys. Rev. B **85**, 035409 (2012).

[87] C. Voinea, S. Pu, A. C. Balram, and Z. Papić, Entanglement scaling and charge fluctuations in a Fermi liquid of composite fermions, Phys. Rev. B **111**, 115119 (2025).

[88] J. Zak, Berry's phase for energy bands in solids, Phys. Rev. Lett. **62**, 2747 (1989).

[89] D. Xiao, M.-C. Chang, and Q. Niu, Berry phase effects on electronic properties, Rev. Mod. Phys. **82**, 1959 (2010).

[90] V. W. Scarola, Wave-function vortex attachment via matrix products: Application to atomic Fermi gases in flat spin-orbit bands, Phys. Rev. B **89**, 115136 (2014).

[91] G. Moore and N. Read, Nonabelions in the fractional quantum Hall effect, Nucl. Phys. B **360**, 362 (1991).

[92] K. K. Ma, M. R. Peterson, V. Scarola, and K. Yang, Fractional quantum Hall effect at the filling factor $\nu = 5/2$, in *Encyclopedia of Condensed Matter Physics*, edited by T. Chakraborty, 2nd ed. (Academic Press, Oxford, U.K., 2024).

[93] M. Levin and X.-G. Wen, Detecting topological order in a ground state wave function, Phys. Rev. Lett. **96**, 110405 (2006).

[94] A. Kitaev and J. Preskill, Topological entanglement entropy, Phys. Rev. Lett. **96**, 110404 (2006).

[95] A. M. Läuchli, E. J. Bergholtz, and M. Haque, Entanglement scaling of fractional quantum Hall states through geometric deformations, New J. Phys. **12**, 075004 (2010).

[96] J. Fröhlich and B. Pedrini, New applications of the chiral anomaly, in *Mathematical Physics 2000* (World Scientific, Singapore, 2000).

[97] S.-C. Zhang and J. Hu, A four-dimensional generalization of the quantum Hall effect, Science **294**, 823 (2001).

[98] H. Sable, S. Das, and V. Scarola, Data for manuscript titled "Quantum Hall correlations in tilted extended Bose-Hubbard chains" [Dataset], Zenodo (2026), https://doi.org/10.5281/zenodo.18234720.